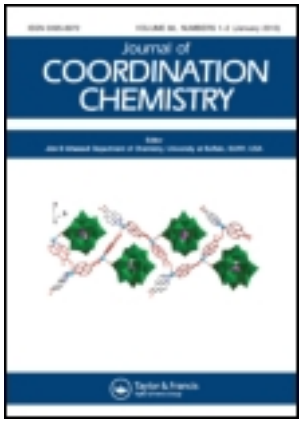

Journal of Coordination Chemistry
Publication details, including instructions for authors and subscription information:
http://www.tandfonline.com/loi/gcoo20

Synthesis and structure of a new polyoxometalate-based inorganic-organic hybrid and application as a chemically bulk-modified electrode

Shenghua Yang [a], Xiangqian Dong [a], Yanping Zhang [a], Huaiming Hu [a] & Ganglin Xue [a]

[a] Key Laboratory of Synthetic and Natural Functional Molecule Chemistry (Ministry of Education), College of Chemistry & Materials Science, Northwest University, Xi'an, China

Accepted author version posted online: 20 Mar 2013.Published online: 19 Apr 2013.

To cite this article: Shenghua Yang, Xiangqian Dong, Yanping Zhang, Huaiming Hu & Ganglin Xue (2013) Synthesis and structure of a new polyoxometalate-based inorganic-organic hybrid and application as a chemically bulk-modified electrode, Journal of Coordination Chemistry, 66:9, 1529-1537, DOI: 10.1080/00958972.2013.786831

To link to this article: http://dx.doi.org/10.1080/00958972.2013.786831

Journal of Coordination Chemistry, 2013
Vol. 66, No. 9, 1529–1537, http://dx.doi.org/10.1080/00958972.2013.786831

Synthesis and structure of a new polyoxometalate-based inorganic–organic hybrid and application as a chemically bulk-modified electrode

SHENGHUA YANG, XIANGQIAN DONG, YANPING ZHANG, HUAIMING HU and GANGLIN XUE*

Key Laboratory of Synthetic and Natural Functional Molecule Chemistry (Ministry of Education), College of Chemistry & Materials Science, Northwest University, Xi'an, China

(*Received 24 September 2012; in final form 17 January 2013*)

A new Keggin-type polyoxometalate-based inorganic–organic hybrid, $[Cu(H_2O)_2(daphen)]_2[SiW_{12}O_{40}]\cdot 9H_2O$ (**1**) (daphen = 5,6-diamino-1,10-phenanthroline), was hydrothermally synthesized, and characterized by single-crystal X-ray diffraction, elemental analysis, infrared spectroscopy, fluorescence spectra, and thermal analysis. Single-crystal X-ray diffraction analysis reveals that in **1**, $[SiW_{12}O_{40}]^{4-}$ is a tetradentate ligand with its four terminal oxygens coordinating to four Cu(II)–daphen fragments to form a 2D sheet with (4,4) topology. On the basis of the insolubility of **1** in water and common organic solvent and its reversible multielectron redox processes, **1** was used to fabricate a bulk-modified carbon paste electrode (**1**-CPE) by direct mixing. Electrochemistry indicated that **1**-CPE is stable over hundreds of cycles and possessed electrocatalytic activity toward the reduction reactions of nitrite.

Keywords: Polyoxometalate; Inorganic–organic hybrid; Electrochemical property

1. Introduction

Versatile structures and potential applications in catalysis, medicine, sorption, magnetism, and photochemistry [1–3] make design and synthesis of inorganic–organic hybrid materials based on polyoxometalates (POMs) of interest [4–6]. The key to the synthesis lies in selection of POMs as building blocks and suitable transition-metal (TM) complexes as structure-directing and functional components [7–10]. Due to size suitability and structure stability, Keggin-type POMs have been mostly employed as structural units to construct inorganic–organic hybrids through linking with TM complexes [11–18]. To date, many N-containing ligands have been used for this purpose, and a variety of one-, two-, and three-dimensional (1D, 2D, and 3D) compounds based on Keggin polyanions and TM complexes, especially Cu complexes, have been reported, such as $[Cu_2(btb)_2(PMo_{12}O_{40})]$ (btb = 1,4-bis(1,2,4-triazol-1-y1)butane) [19], $[Cu^{I}_3(L1)_3][PW_{12}O_{40}]$ (L = 1,4-bis(pyrazol-1-ylmethyl)benzene) [20], $[Cu_2(L)_4(H_2O)_2](SiW_{12}O_{40})\cdot 8H_2O$ (L = 1,1′-(1,4-but-anediyl)

*Corresponding author. Email: glxue@nwu.edu.cn

bis-1H-benzimidazole) [21], $[Cu^{I}_5(btx)_4(PW^{VI}_{10}W^{V}_2O_{40})]$ and $[Cu^{II}_2(btx)_4(SiW_{12}O_{40})]$ (btx = 1,6-bis(1,2,4-triazol-1-y1)hexane) [22], $[Cu(py)_2]_4[SiW_{12}O_{40}]$ (py = pyridine) [23], $(H_3O)[Cu^{I}(4,4'\text{-bipy})]_3[SiW_{12}O_{40}]\cdot 1.5H_2O$ [24], $[\{Cu(phen)_2\}_2SiW_{12}O_{40}]$ [25], and $[Cu_4bmtm)_4][SiW_{12}O_{40}]\cdot 3H_2O$, $[Cu_4(bmte)_{3.5}][SiW_{12}O_{40}]$ and $[Cu_4(bmtp)_4][SiW_{12}O_{40}]$ [bmtm = 1,1′-bis(1-methyl-5-mercapto-1,2,3,4-tetrazole)methane, bmte = 1,2-bis(1-methyl-5-mercapto-1,2,3,4-tetrazole)-ethane, and bmtp = 1,5-bis(1-methyl-5-mercapto-1,2,3,4-tetrazole)pentane] [26], etc. Recently, Chen *et al.* reported the first example of a POM-based hybrid compound that contains daphen, $Cu_2(daphen)_2(H_2O)_4(PW_{11}W^{V}O_{40})]\cdot 6H_2O$ [27]. The self-assembly process is very complicated, affected by subtle changes, such as reactants, pH, temperature, and reaction time [28, 29]. Thus, exploring the synthetic rules for self-assembly of POM-based hybrid materials is challenging and meaningful. In this paper, choosing $[SiW_{12}O_{40}]^{4-}$ and 5,6-diamino-1,10-phenanthroline, under hydrothermal conditions, we obtained a new POM-based coordination polymer $[Cu(H_2O)_2(C_{12}H_{10}N_4)]_2[SiW_{12}O_{40}]\cdot 9H_2O$ (**1**), which was further used as a solid material to fabricate a bulk-modified carbon paste electrode on the basis of the insolubility of 1 in water and common organic solvents and its reversible multielectron redox processes. Electrochemistry indicated that carbon paste electrode (**1**-CPE) is stable over hundreds of cycles and has electrocatalytic activities toward reduction of nitrite.

2. Experimental

2.1. *Materials and methods*

All reagents were purchased commercially and used without purification. $K_4[\alpha\text{-}SiW_{12}O_{40}]\cdot 17H_2O$ was prepared by the method reported. Elemental analyses (C, H, and N) were performed on a Perkin-Elmer 2400 CHN elemental analyzer. FT-IR spectra were obtained on a 55 EQUINOX55 IR spectrometer with KBr pellets. Thermal analysis was performed on a STA449C integration thermogravimetric (TG) analyzer under N_2 with a heating rate of 10 °C min^{-1} from 30 to 700 °C. A CHI 660 Electrochemical Workstation connected to a Digital-586 personal computer was used for control of the electrochemical measurements and for data collection. A conventional three-electrode system was used. A saturated calomel reference electrode (SCE) and Pt gauze as a counter electrode were used. The title compound chemically bulk-modified CPEs was used as the working electrode.

2.2. *Synthesis of $[Cu(H_2O)_2(C_{12}H_{10}N_4)]_2SiW_{12}O_{40}\cdot 9H_2O$ (1)*

$K_4[\alpha\text{-}SiW_{12}O_{40}]\cdot 17H_2O$ (0.67 g, 0.2 mmol), $CuCl_2\cdot 2H_2O$ (0.08 g, 0.4 mmol), and 1,10-phenanthroline-5,6-diamine (0.08 g, 0.4 mmol) were dissolved in 10 mL of distilled water and stirred for 45 min. The pH of the mixture was adjusted to 6.0 and then sealed in a 25 mL Teflon-lined autoclave. After heating at 170 °C for 48 h, the reactor was slowly cooled to room temperature. Yellow-green crystals of **1** were obtained in 75% yield based on W. Elemental Anal. Calcd for $C_{24}H_{46}N_8Cu_2SiW_{12}O_{53}$ (%): C, 7.88; Si, 0.7; N, 3.1; Cu, 1.7; W, 60.3. Found: C, 8.02; Si, 0.81; N, 3.3; Cu, 1.8; W, 60.5.

2.3. *Preparation of 1 bulk-modified carbon paste electrode*

The **1** bulk-modified **1**-CPE was fabricated as follows: 0.50 g graphite powder and 0.02 g of **1** were mixed and ground together by agate mortar and pestle to achieve a uniform

mixture; then 0.10 mL of paraffin oil was added with stirring. The homogenized mixture was packed into a glass tube of 2 mm inner diameter, and the surface of the modified CPE was wiped with weighing paper, and electrical contact was established with a copper rod through the back of the electrode. The same procedure was used for preparation of bare CPE without **1**.

2.4. *X-ray crystallography*

A selected crystal of **1** was mounted on a glass fiber capillary which was put on a BRUKER SMART APEX II CCD diffractometer equipped with graphite monochromated radiation used for data collection. Data were collected at 296(2) K using Mo$K\alpha$ radiation ($\lambda = 0.71073$ Å). The structure was solved by direct methods (SHELXTL-97) and refined by full-matrix-block least-squares on F^2. All nonH atoms were refined anisotropically except half-occupied oxygens around the central Si of $SiW_{12}O_{40}^{4-}$, and these disordered oxygens were refined isotropically. The positions of hydrogens on C or N were calculated theoretically. Hydrogens of water were not included. A summary of the crystal data and structure refinements for **1** is given in table 1. Selected bond lengths and angles are listed in table S1. The CCDC reference number is CCDC 902374 for **1**.

3. Results and discussion

3.1. *Structure description*

Compound **1** crystallizes in the monoclinic space group $P2(1)/n$ and the asymmetric unit of **1** contains half of $[SiW_{12}O_{40}]^{4-}$, one $[Cu(H_2O)_2(C_{12}H_{10}N_4)]^{2+}$, and four-and-half water molecules (figure S1). The central Si in the Keggin ion exhibits the same type of crystallographic disorder as found in many other crystal structures with Keggin anions [27], the central Si is

Table 1. Crystal data and structure refinement for **1**.

Formula	$C_{24}H_{46}N_8Cu_2O_{53}SiW_{12}$
Formula weight	3656.06
T/K	296
Crystal system	Monoclinic
Space group	$P2(1)/n$
a/Å	11.579(5)
b/Å	19.504(9)
c/Å	14.642(6)
α/°	90.00
β/°	106.576(7)
γ/°	90.00
V/Å^3	3169(2)
Z	2
d_{Calcd}/g cm^{-3}	3.831
μ/mm^{-1}	22.469
Reflections measured	14,993
Independent reflections	5437
Reflections used	4806
R_{int}	0.0492
GoF on F^2	1.012
$R1$ [$I > 2\sigma(I)$][a], $wR2$ [$I > 2\sigma(I)$][b]	0.0541, 0.1315
$R1$ [(all data)][a], $wR2$ (all data)[b]	0.0624, 0.1367
Diff. peak and hole, e A^{-3}	2.373, −2.431

[a]$R1 = [\Sigma|F_o| - |F_c|]/[\Sigma|F_c|]$. [b]$wR2 = \{[\Sigma w(F_o^2 - F_c^2)^2]/[\Sigma w(F_o^2)^2]\}^{1/2}$.

surrounded by a cube of eight oxygens with each oxygen site half-occupied, and the Si and these oxygens formed two tetrahedra. The central Si-O distances of polyoxoanion vary from 1.57(2) to 1.60(2) Å, and the distances of W-O bonds are divided into three groups: W-O_c(central), 2.38(2)–2.42(2) Å, W-O_b(bridge), 1.85(2)–1.95(2) Å, and W-O_t(terminal), 1.66(2)–1.71(2) Å, in which the distance of W-O_t···Cu is the longest. All other bond lengths and angles are normal and consistent with those reported in the literature [30]. Cu1 is coordinated by two nitrogens from one 1,10-phenanthroline-5,6-diamine with Cu–N bond distances of 1.977(19) and 1.98(2) Å, two oxygens of two coordination water molecules with Cu–O_W bond distances of 1.983(18) and 1.967(18) Å, and two terminal oxygens of $[SiW_{12}O_{40}]^{4-}$ with Cu–O bond distances of 2.387(15) and 2.35(2) Å, showing a distorted

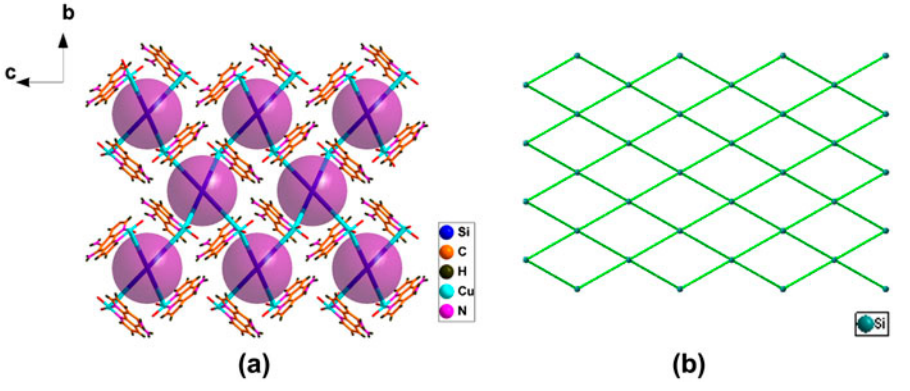

Figure 1. (a) The 2D framework of **1**. (b) Schematic view of the layer with (4,4) topology. Color code: Gray blue ball: $[SiW_{12}O_{40}]^{4-}$ anion (see http://dx.doi.org/10.1080/00206814.2013.786831 for color version).

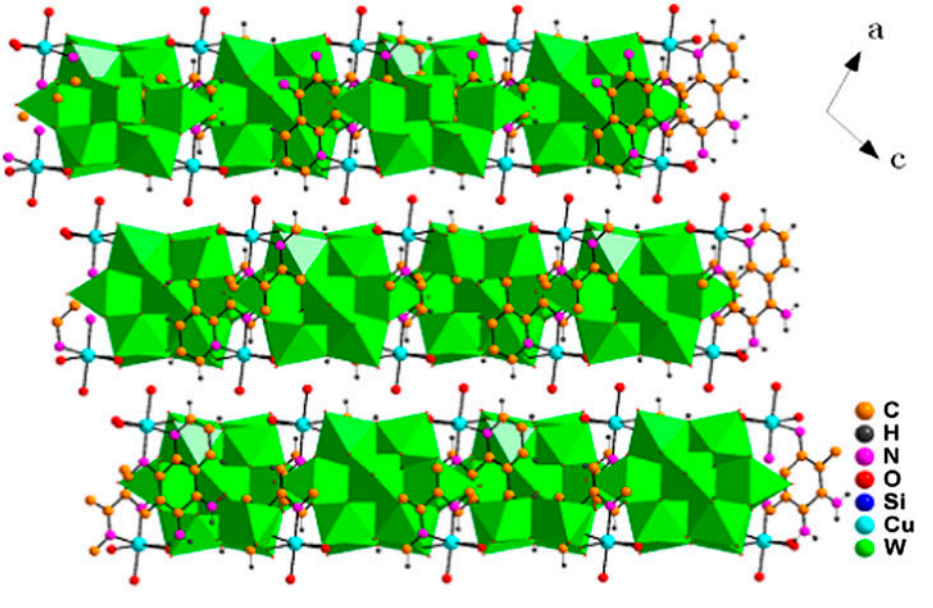

Figure 2. The packing arrangement of the compound along the *b* direction. The isolated water molecules are omitted for clarity.

octahedral geometry due to strong Jahn–Teller distortion [31]. In **1**, $[SiW_{12}O_{40}]^{4-}$ is tetradentate coordinating four Cu^{2+} ions by terminal oxygens; each $[Cu(H_2O)_2(C_{12}H_{10}N_4)]^{2+}$ is connected with two $[SiW_{12}O_{40}]^{4-}$ polyoxoanions, leading to a 2D sheet with (4,4) topology (figure 1).

The packing arrangement of **1** along the *b* direction is shown in figure 2. Adjacent 2D layers are further packed into 3D supramolecular assemblies through hydrogen bonds among ligand water, lattice water, nitrogen on the daphen, and oxygens of $[SiW_{12}O_{40}]^{4-}$. Typical hydrogen bonds are as follows: O10···O24 W 2.94 Å, O26 W···O24 W 2.54 Å, N4···O29 W 2.86 Å, N3···O28 W 2.98 Å, O27 W···O29 W 2.63 Å, O7···O24 W 2.96 Å.

3.2. *FT-IR spectrum*

The IR spectrum (figure S2) of **1** exhibits four characteristic absorptions of the Keggin $[SiW_{12}O_{40}]^{4-}$ anion, peaks at 1020, 974, and 795 cm^{-1} attributed to $\nu(Si–O_a)$, $\nu(W–O_t)$, and $\nu(W–O_c–W)$, respectively, that at 922 cm^{-1} to overlapping infrared absorbance of $\nu(W–O_c–W)$ and $\nu(Si–O_a)$, which are comparable with 1032, 923, 968, and 792 cm^{-1} of $[Cu_2(L)_4(H_2O)_2](SiW_{12}O_{40})\cdot 8H_2O$ [L = 1,1′-(1,4-butanediyl)bis-1H-benzimidazole [21]]; 918, 964, 877, and 779 cm^{-1} for $\{(H_3O)[Cu^{I}(4,4'\text{-bipy})]_3[SiW_{12}O_{40}]\}\cdot 1.5H_2O$ [24]; and 920, 971, 850, and 790 cm^{-1} for $[\{Cu(phen)_2\}_2SiW_{12}O_{40}]$ [25].

3.3. *Fluorescence*

Emission spectra of **1** and $K_4[SiW_{12}O_{40}]\cdot 17H_2O$ in the solid state at room temperature are compared in figure 3. $K_4[SiW_{12}O_{40}]\cdot 17H_2O$ shows two broad emission peaks at 398 and 452 nm, assigned to O2p to W4d charge transfer upon excitation at 240 nm; however, the two emission bands in **1** exhibit redshift, located at ca. 405 and 454 nm, and the emission intensity of $K_4[SiW_{12}O_{40}]\cdot 17H_2O$ is much stronger than that of **1**, caused by the strong interaction between the $[SiW_{12}O_{40}]^{4-}$ anion and $[Cu(H_2O)_2(C_{12}H_{10}N_4)]^{2+}$.

3.4. *Thermogravimetric analyses*

The TG-DSC curves of **1** (figure S3) show that its thermal decomposition can be divided into two steps. The first weight loss of 6.5% occurs between 30 and 280 °C, corresponding

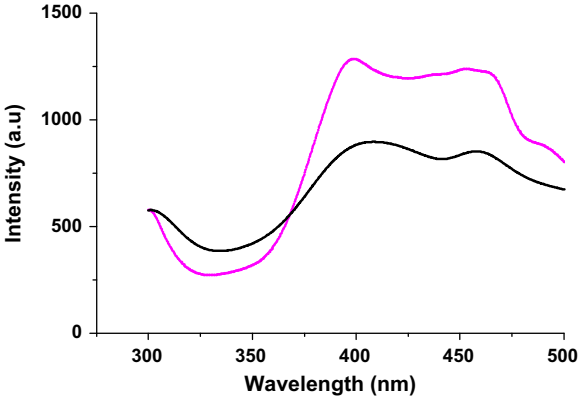

Figure 3. Fluorescence spectra of **1** and $K_4[SiW_{12}O_{40}]\cdot 17H_2O$. The line code is as follows: compound **1** (——) and $K_4[SiW_{12}O_{40}]\cdot 17H_2O$ (- - -).

to the loss of nine lattice and four coordinated water molecules (Calcd 6.4%). The second weight loss of 11.6% from 280 to 680 °C is assigned to decomposition of the polyanion framework structure with release of two 1,10-phenanthroline-5,6-diamine (Calcd 11.5%). The observed total weight loss (18.1%) is in agreement with the calculated value (17.9%) and the remaining residues correspond to the mixed oxides $2CuO{\cdot}SiO_2{\cdot}12WO_3$. Accordingly, the DSC curve shows two endothermic peaks at 184 and 515 °C.

3.5. *Electrochemical behavior of 1-CPE*

Electrochemical studies were carried out in 1 M H_2SO_4 aqueous solution. figure 4 presents the cyclic voltammograms of **1**-CPE from +800 to −500 mV at 200 mV s^{-1}. There exist five pairs of redox peaks (I-I′, II-II′, Ш-Ш′, IV-IV′, and V-V′) with the mean potentials $E_{1/2} = (E_{pc} + E_{pa})/2$ of +421, +220, +5, −284, and −414 mV (*vs.* SCE), respectively. The last three redox peaks from −500 to 10 mV can be ascribed to redox of $[SiW_{12}O_{40}]^{4-}$, while the other two can be ascribed to redox of Cu^{2+}.

The electrochemical behaviors of **1**-CPE are comparable with those of $[\{K(C_6H_{10}N_2O_2S)_2(H_2O)\}_2(SiW_{12}O_{40})_2]{\cdot}2H_3O{\cdot}10H_2O$, and the cyclic voltammogram in 10^{-3} mol L^{-1} ($CH_3COONa + CH_3COOH$) buffer solution (pH 5.0) showed four reversible redox peaks with mean potentials of +481, −182, −428, and −626 mV, respectively [32]. The CPE fabricated from $[Cu^{II}_2(btx)_4(SiW_{12}O_{40})]$ (btx = 1,6-bis(1,2,4-triazol-1-yl)hexane) under similar condition [22] only exhibited two reversible redox peaks with the mean potentials at −449 and −614 mV, respectively, ascribed to the last two redox processes of SiW_{12}. We can see that the potential of the first redox pair $E_{1/2}$ of SiW_{12} for **1**-CPE is more positive, which may relate to the stronger combination of Cu complex with SiW_{12} in **1**.

figure 5 shows the cyclic voltammograms of **1**-CPE at different scan rates in 1 M H_2SO_4 from +800 to −500 mV. When the scan rate is varied from 40 to 380 mV s^{-1}, the cathodic peak potentials shift negative whereas the corresponding anodic peak potentials shift positive, and the peak currents increase along with rising scan rates. For II-II′ redox process, the peak currents were proportional to the scan rates when the scan rates are lower than 120 mV s^{-1} (figure S4), which indicates that the redox process is surface

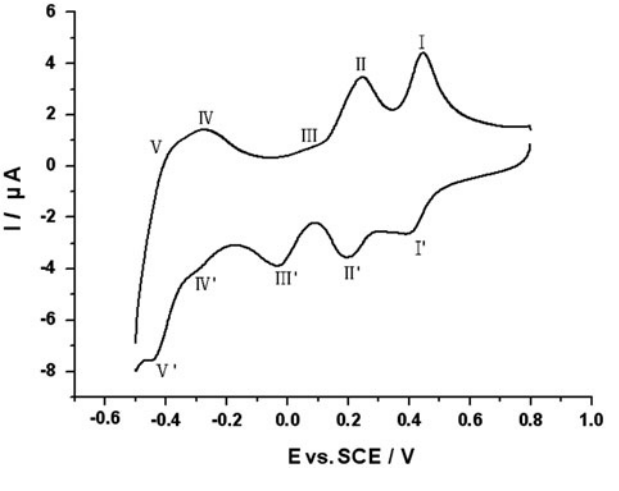

Figure 4. The cyclic voltammograms of **1**-CPE in 1 M H_2SO_4. Scan rate: 200 mV s^{-1}.

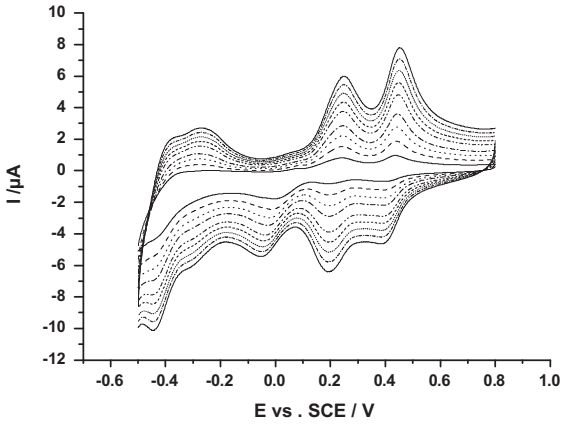

Figure 5. The cyclic voltammograms of **1**-CPE in 1 M H_2SO_4 at different scan rates from inner to outer: 40, 80, 120, 160, 220, 260, 300, 340, and 380 mV s^{-1}.

controlled and the exchanging rate of electrons is fast; however, when the scan rates were higher than 120 mV s^{-1}, the peak currents were proportional to the square root of the scan rate (figure S5), indicating that the redox process is diffusion controlled. The peak-to-peak separations between the corresponding cathodic and anodic peaks decrease with the scan rate due to internal resistance loss caused by resistance of the composite.

3.6. *Electrocatalytic activity of 1-CPE for reduction of nitrite*

The electrocatalytic reduction of **1**-CPE toward nitrite in 1 M H_2SO_4 aqueous solution in the potential range of +800 to −500 mV is shown in figure 6. Direct electroreduction of nitrite requires a large overpotential at most electrode surfaces and no obvious response was observed at a bare CPE in the potential range in 1 M H_2SO_4 aqueous solution containing some KNO_2, while **1**-CPE exhibits a good electrocatalytic activity toward the reduction of nitrite. With the addition of nitrite, the reduction peak currents of Cu^{2+} centers are

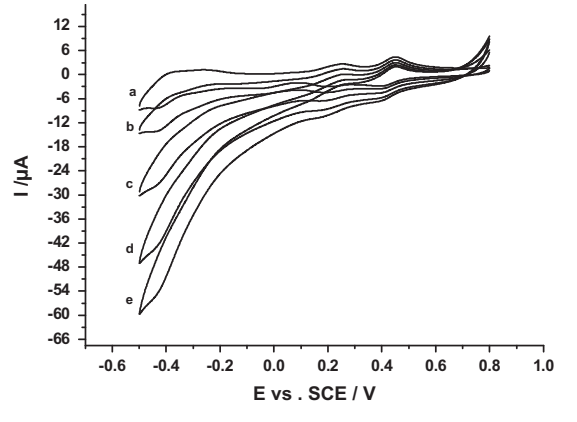

Figure 6. The cyclic voltammograms of **1**-CPE in 1 M H_2SO_4 containing 0 (a); 2 (b); 4 (c); 6 (d); and 8 (e) mM $NaNO_2$. Scan rate: 100 mV s^{-1}.

almost unaffected. However, all the reduction peak currents of $[SiW_{12}O_{40}]^{4-}$ polyanions increase markedly while the corresponding oxidation peak currents decrease, suggesting that reduction of nitrite is mediated by reduced species of $[SiW_{12}O_{40}]^{4-}$ in **1**.

4. Conclusion

A new inorganic–organic hybrid compound based on $[SiW_{12}O_{40}]^{4-}$ and $[Cu(H_2O)_2(C_{12}H_{10}N_4)]^{2+}$ has been obtained by the hydrothermal method. Compound **1** has a 2D sheet with (4,4) topology templated by $[SiW_{12}O_{40}]^{4-}$ polyanions. In view of the insolubility of **1** in water and common organic solvent and its reversible multielectron redox processes, it was used as a solid to fabricate a bulk-modified **1**-CPE, and the electrocatalysis behavior of **1**-CPE was investigated; **1**-CPE is a good catalyst for nitrite.

Acknowledgment

This work was supported by the National Natural Science Foundation of China (20973133).

References

[1] D.E. Katsoulis. *Chem. Rev.*, **98**, 359 (1998).
[2] A. Dolbecq, E. Dumas, C.R. Mayer, P. Mialane. *Chem. Rev.*, **110**, 6009 (2010).
[3] D.-L. Long, R. Tsunashima, L. Cronin. *Angew. Chem. Int. Ed.*, **49**, 1736 (2010).
[4] A. Muller, S. Shah, H. Bogge, M. Schmidtmann. *Nature*, **397**, 48 (1999).
[5] A.E. Kuznetsov, Y.V. Geletii, C.L. Hill, K. Morokuma, D.G. Musaev. *J. Am. Chem. Soc.*, **131**, 6844 (2009).
[6] H.-Y. An, E.-B. Wang, D.-R. Xiao, Y.-G. Li, Z.-M. Su, L. Angew. *Chem. Int. Ed.*, **45**, 904 (2006).
[7] H. Zhang, L.Y. Duan, Y. Lan. *Inorg. Chem.*, **42**, 8053 (2003).
[8] J. Li, Y.-G. Chen, C.-J. Zhang. *J. Mol. Struct.*, **921**, 233 (2009).
[9] Y. Wang, D.R. Xiao, E.B. Wang, L.L. Fan, J. Liu. *Transition Met. Chem.*, **32**, 950 (2007).
[10] Z.-H. Yi, X.-B. Cui, X. Zhang, G.-D. Yang, J.-Q. Xu, X.-Y. Yu, H.-H. Yu, W.-J. Duan. *J. Mol. Struct.*, **891**, 123 (2008).
[11] G.G. Gao, P.S. Cheng, T.C.W. Mak. *J. Am. Chem. Soc.*, **131**, 18257 (2009).
[12] H.Q. Tan, Y.G. Li, Z.M. Zhang, C. Qin, X.L. Wang, E.B. Wang, Z.M. Su. *J. Am. Chem. Soc.*, **129**, 10066 (2007).
[13] T.B. Liu, B. Imber, E. Diemann, G. Liu, K. Cokleski, H.L. Li, Z.Q. Chen, A. Müller. *J. Am. Chem. Soc.*, **128**, 15914 (2006).
[14] H. Imai, T. Akutagawa, F. Kudo, M. Ito, K. Toyoda, S. Noro, L. Cronin, T. Nakamura. *J. Am. Chem. Soc.*, **131**, 13578 (2009).
[15] C.P. Pradeep, D.L. Long, C. Streb, L. Cronin. *J. Am. Chem. Soc.*, **130**, 14946 (2008).
[16] D.L. Long, E. Burkholder, L. Cronin. *Chem. Soc. Rev.*, **36**, 105 (2007).
[17] S. Shishido, T. Ozeki. *J. Am. Chem. Soc.*, **130**, 10588 (2008).
[18] C. Ritchie, E.M. Burkholder, D.L. Long, D. Adam, P. Kögerler, L. Cronin. *Chem. Commun.*, **468**, (2007).
[19] A.-X. Tian, J. Ying, J. Peng, J.-Q. Sha, H.-J. Pang, P.-P. Zhang, Y. Chen, M. Zhu, Z.-M. Cryst. *Growth Des.*, **8**, 10 (2008).
[20] G.-F. Hou, L.-H. Bi, B. Li, L.-X. Inorg. *Chemistry*, **49**, 14 (2010).
[21] X.-L. Wang, J. Li, H.-Y. Lin, G.-C. Liu, A.-X. Tian, H.-L. Hu, X.-J. Liu, Z.-H. Kang. *J. Mol. Struct.*, **983**, 99 (2010).
[22] A.-X. Tian, X.-L. Lin, Y.-J. Liu, G.-Y. Liu, J. Ying, X.-L. Wang, H.-Y. Lin. *J. Coord. Chem.*, **65**, 2147 (2012).
[23] R. Yang, S.-X. Liu, Q. Tang, S.-J. Li, D.-D. Liang. *J. Coord. Chem.*, **65**, 891 (2012).
[24] J.-F. Cao, S.-X. Liu, Y.-H. Ren, R.-G. Cao, C.-Y. Gao, X.-Y. Zhao, L.-H. Xie. *J. Coord. Chem.*, **62**, 1381 (2009).
[25] F.-X. Meng, J. Sun, K. Liu, F.-X. Ma, Y.-G. Chen. *J. Coord. Chem.*, **60**, 401 (2007).
[26] X.-L. Wang, H.-L. Hu, A.-X. Tian, H.-Y. Lin, J. Li. *Inorg. Chem.*, **49**, 10299 (2010).

[27] Q.-J. Kong, M.-X. Hu, Y.-G. Chen. *J. Coord. Chem.*, **64**, 3237 (2011).
[28] Y.Q. Lan, S.L. Li, X.L. Wang, K.Z. Shao, D.Y. Du, H.Y. Zang, Z. Inorg. *Chemistry*, **47**, 8179 (2008).
[29] J.X. Meng, Y. Lu, Y.G. Li, H. Fu, E.B. Wang. *Cryst. Growth Des.*, **9**, 4116 (2009).
[30] (a) H.T. Evans Jr., M.T. Pope. Inorg. Chem., 23, 501 (1984); (b) D. Attanasio, M. Bonamico, V. Fares, P. Imperatori, L. Suber. J. Chem. Soc., Dalton Trans., 3221 (1990).
[31] T.J.R. Weakley, R.G. Finke. *Inorg. Chem.*, **29**, 1235 (1990).
[32] J. Wu, C.-X. Wang, K. Yu, Z.-U. Su, Y. Yu, Y.-L. Xu, B.-B. Zhou. *J. Coord. Chem.*, **65**, 69 (2012).